RSC Advances

PAPER

View Article Online
View Journal | View Issue

Cite this: *RSC Adv.*, 2022, **12**, 20251

Enhancing the quantum yield of singlet oxygen: photocatalytic degradation of mustard gas simulant 2-chloroethyl ethyl sulfide catalyzed by a hybrid of polyhydroxyl aluminum cations and porphyrin anions†

Ying Yang,[ab] Jianbo Yin,[a] Fangsheng Tao,[a] Yunshan Zhou, *[a] Lijuan Zhang,*[a] Yuxu Zhong*[b] and Yong'an Wang[b]

By combining the anionic salt meso-tetra(4-carboxyphenyl)porphyrin ($TCPP^{4-}$) and the Keggin polyoxometalate cation cluster $[Al_{13}O_4(OH)_{24}(H_2O)_{12}]^{7+}$ *via* a simple ion-exchange method, a hybrid $(C_{48}H_{26}N_4O_8)[Al_{13}O_4(OH)_{24}(H_2O)_{12}]_2(OH)_{10}\cdot 18H_2O$ (Al_{13}–TCPP) was prepared and thoroughly characterized as a prototype of polyoxometalate–porphyrin hybrids for the photocatalytic degradation of the mustard gas simulant 2-chloroethyl ethyl sulfide (CEES). The experimental results showed that the catalytic degradation rate of CEES in the presence of Al_{13}–TCPP reached 96.16 and 99.01% in 180 and 90 min in methanol and methanol–water solvent mixture (v/v = 1 : 1), respectively. The reaction followed first-order reaction kinetics, and the half-life and kinetic constant in methanol and solvent mixture were 39.8 min, $-0.017\ min^{-1}$ and 14.7 min, $-0.047\ min^{-1}$. Mechanism analysis indicated that under visible light irradiation in air, CEES was degraded through a combination of oxidation and alcoholysis/hydrolysis in methanol and the methanol–water solvent mixture. The superoxide radical ($O_2^{\bullet -}$) and singlet molecular oxygen ($^1O_2$) generated by Al_{13}–TCPP selectively oxidized CEES into a non-toxic sulfoxide. The singlet oxygen capture experiments showed that Al_{13}–TCPP (Φ = 0.236) had a higher quantum yield of singlet oxygen generation than H_4TCPP (Φ = 0.135) under visible light irradiation in air. The material Al_{13}–TCPP has good reusability, and the degradation rate of CEES can still reach 98.37% after being recycled five times.

Received 21st March 2022
Accepted 30th June 2022

DOI: 10.1039/d2ra01821g

rsc.li/rsc-advances

Introduction

Mustard gas (HD) can severely damage the respiratory tract, surface skin and other parts in humans, and thus poses a great threat to the safety of human life.[1] Currently, the degradation of HD is mainly achieved through hydrolysis, elimination, oxidation and other reactions.[2] The greatest disadvantage of the first two methods is the slow rate of digestion,[2–6] while the oxidation method has the risk of over-oxidation to produce mustard sulfone, which has an equivalent toxicity to HD.[7,8] Singlet molecular oxygen ($^1O_2$) has mild oxidizability and can selectively oxidize HD/CEES to a non-toxic sulfoxide product.[8–11] Therefore, the oxidative degradation of HD by $^1O_2$ has attracted considerable attention in recent years.

Porphyrin has a large π-conjugated electronic structure, a high absorption in the visible-near infrared region, and its structure is easily adjusted. As a commonly used photosensitizer, porphyrin has the ability to convert O_2 in the inert triplet ground state ($^3O_2$) into the active $^1O_2$.[10,12] Porphyrin is widely used in photodynamic therapy[13] and photocatalysis.[14,15] However, the ability of $^1O_2$ production from porphyrin is limited due to the easy self-aggregation of porphyrin molecules in solvents.[16,17] In order to solve this problem, some efforts have been tried, *e.g.*, fix porphyrin molecules on the surface of a carrier through coordination bonds to prevent their self-aggregation,[18] obtain porphyrin nanoparticles[19] through a limited non-covalent self-assembly process, and covalently link porphyrin with (oxo)metal units to form highly periodically isolated and dispersed porphyrin–metal–organic framework compounds.[9,10,20–24] These efforts lead to a greatly increased quantum yield of $^1O_2$ by porphyrin, and further improving the performance of porphyrin-based materials in the selective oxidation of mustard gas simulant CEES to sulfoxide under

[a]*State Key Laboratory of Chemical Resource Engineering, College of Chemistry, Beijing University of Chemical Technology, Beijing 100029, P. R. China. E-mail: zhouys@mail.buct.edu.cn*

[b]*Toxicology and Medical Countermeasures, Beijing Institute of Pharmacology and Toxicology, Beijing 100850, P. R. China*

† Electronic supplementary information (ESI) available. See https://doi.org/10.1039/d2ra01821g

visible light irradiation. In this scenario, polyoxometalates, a class of metal oxygen clusters linked by central atoms and metal atoms (such as V, W and Mo, *etc.*[25–27]) and oxygen atoms,[28,29] have a wide range of practical/potential applications in various fields[30–33] can also be used for CEES decontamination, such as PMo_{12}@PDDA-rGO[34] and $SiW_{10}Cu_2$/GO.[35] Notably, the reported porphyrin–polyoxometalate hybrids show more efficient photocatalytic oxidation ability for alcohols[31] and rhodamine[36] than porphyrins. The combination of polyoxometalate and porphyrin has a potential to take advantage of not only both the two individual components but also their possible cooperativity/synergistic effect to increase the $^1O_2$ and $O_2^{\bullet-}$ yield of porphyrin, which can be used in the selective oxidation of HD/CEES. Due to the oleophilic nature of CEES, its low solubility in pure water limits its hydrolysis rate in water. The mixture of organic solvents and water has been proved to increase the solubility of CEES in solvents and increase the hydrolysis rate.[37,38] In addition, using protic solvent can effectively improve the selectivity of CEESO formation.[39–41] Therefore, methanol and methanol–water mixture were selected as solvents for research.

Based on the above analysis, the photosensitive anionic salt meso-tetra (4-carboxyphenyl) porphyrin ($TCPP^{4-}$) was selected to combine with the Keggin-type polyoxometalate $[Al_{13}O_4(OH)_{24}(H_2O)_{12}]^{7+}$ cationic metal cluster to synthesize a new polyhydroxyl aluminum cationic cluster-porphyrin anion hybrid as a prototype of porphyrin–polyoxometalate hybrids for the photocatalytic degradation of HD/CEES. As expected, this material can efficiently and selectively digest CEES in methanol and methanol–water solvent mixture due to generated $O_2^{\bullet-}$ and $^1O_2$ under visible light irradiation in air.

Experimental section

Instruments and reagents

The chemicals and reagents used in this study are analytically pure and used as received without further purification. Aluminum chloride hexahydrate ($AlCl_3 \cdot 6H_2O$, 99%) and sodium hydroxide (98%) were purchased from Beijing Chemical Reagent Co., Ltd (Beijing, China). Pyrrole (99%), *p*-formylbenzoic acid (98%), and 1-benzoquinone (98%) was purchased from Shanghai Aladdin Reagent Co., Ltd (Shanghai, China). 9,10-Diphenylanthracene (98%) and nitroblue tetrazolium (98%) were purchased from Beijing Yancheng Technology Co., Ltd (Beijing, China). Glacial acetic acid, dimethyl sulfoxide (DMSO), dichloromethane and propionic acid were purchased from Beijing Chemical Plant (Beijing, China). Methanol was obtained from Tianjin Siyou Fine Chemicals Co., Ltd (Tianjin, China), and 2-chloroethyl ethyl sulfide (95%) was purchased from Beijing Bailingwei Technology Co., Ltd (Beijing, China). Thymol phthalein (98%) was purchased from Beijing Huawei Ruike Chemical Co., Ltd (Beijing, China). The meso-tetra (4-carboxyphenyl) porphyrin (H_4TCPP) was synthesized according to the literature[42] and characterized by Fourier transform infrared (FTIR) spectroscopy and proton nuclear magnetic resonance (^1H NMR) spectroscopy. The ε-$[Al_{13}O_4(OH)_{24}(H_2O)_{12}]^{7+}$ solution and Al_{13}–SO_4 were prepared by a previously reported method[43] (see ESI†).

The chemical synthesis was performed using a CEL-LAB500 Multiposition Photochemical Reaction Apparatus (Beijing Zhongjiao Jinyuan Technology Co., Ltd, Beijing, China) equipped with a PLS-LAX500 long-arc xenon lamp (Beijing Zhongjiao Jinyuan Technology Co., Ltd) as light source. The working voltage was 50 V, the working current was 10 A, and the output power was 500 W. The spectrophotometric analysis was performed on a Shimadzu UV-2550 ultraviolet-visible (UV-visible) spectrophotometer (Shimadzu Corporation, Kyoto, Japan), in the wavelength range of 300–650 nm. Solid-state ^{27}Al NMR spectra were recorded on an Avance AV600 NMR spectrometer (Bruker AXS GmbH, Karlsruhe, Germany). Infrared spectra were collected on an ICAN9 FTIR spectrometer (Tianjin Energy Spectrum Technology Co., Ltd, Tianjin, China), using KBr tablets in the wavenumber range of 400–4000 cm^{-1}. The thermogravimetric derivative thermogravimetric (TG-DTG) analysis were performed on a Netzsch STA449 (Netzsch Gerätebau GmbH, Selb, Germany) using the following test conditions: the air flow temperature rises from 14 °C to 1000 °C at the rate of 10 °C min^{-1}. The elemental analysis was performed using the Elementar Vario EL CUBE Elemental Analyzer (Elementar Analysensysteme GmbH, Hanau, Germany). The chromatography-mass spectrometry (GC-MS) analysis was performed on a Thermo Scientific Trace ISQ™ GC-MS system (Thermo Fisher Scientific Inc., Waltham, MA, USA), using the following test conditions: the size of the TR-WAXMS capillary column was 30 m × 0.25 mm × 0.25 μm; the carrier gas was helium, at the flow rate of 1 mL min^{-1}. The programmed temperature rise parameters were as follows: hold at 40 °C for 3 min, heat to 230 °C at a rate of 20 °C min^{-1}, and hold for 3 min. The injection mode was set to split injection, the temperature of the injection port was set to 220 °C, and the split ratio was adjusted to 1 : 200. The detector was an electron ionization (EI) source, the mass spectrometer ion source temperature was 250 °C, and the transmission line temperature was 230 °C. The X-ray diffraction (XRD) analysis was performed on a Rigaku D/max 2500 X-ray diffractometer (Rigaku Corporation, Tokyo, Japan) using a scanning range from 3–90° at the scanning speed of 10° min^{-1}. The X-ray fluorescence Spectrometer (XRF) analysis was performed on a Shimadzu XRF-1800 (Shimadzu Corporation, Kyoto, Japan).

Preparation of Al_{13}–TCPP

H_4TCPP (98 mg, 0.1 mmol) was dissolved in a 0.1 mol L^{-1} NaOH solution of 30 mL to obtain the sodium salt. Then, the salt was slowly added to the 40 mL of the prepared Al_{13}^{7+} solution, and a precipitate gradually formed during the dripping process. After carefully observing the change of the color of the solution, the dripping was immediately stopped when the color changed from dark green to red. After filtering the solution, the unreacted porphyrin and Al_{13}^{7+} were washed with deionized water until the filtrate became colorless. Subsequently, the filter cake was placed in an 80 °C oven for 8 hours, and eventually a brown–black solid of 310 mg was obtained (yield 92%, based

on H_4TCPP). The CHN elemental analysis and XRF analysis values of ($C_{48}H_{26}N_4O_8$) $[Al_{13}O_4(OH)_{24}(H_2O)_{12}]_2(OH)_{10}\cdot 18H_2O$ were as follows: C: 17.05%, H: 4.71%, N: 1.49%, Al: 22.12%. The theoretical value: C: 17.16%, H: 5.04%, N: 1.67%, Al: 20.90%. IR data (KBr, cm^{-1}): 1597 (s), 1408 (s), 801 (m), 651 (m), 545 (s), 495 (w).

Experimental process of the degradation of CEES

A certain quantity (particle size 500 mesh) catalyst was placed in a 50 mL quartz reaction tube, and 5 mL of methanol or 5 mL of methanol–water solvent mixture (v/v = 1 : 1) was added as the reaction solvent, followed by the addition of 5 μL of CEES. The reaction was started by stirring under a 500 W xenon lamp light source ($\lambda > 400$ nm). At different reaction times, a 100 μL aliquot of the reaction solution was taken from the reaction tube, mixed with 200 μL of blue reagent and 100 μL of absolute ethanol and the solution was then placed in a water bath at 80 °C for 15 min. After cooling to room temperature, 5 μL of acetic acid solution (6 mol L^{-1}) and 3 mL of 95% ethanol were added, and then the absorbance was measured at 445 nm on a UV spectrophotometer. The CEES concentration remaining after the reaction was calculated according to the standard curve (Fig. S1†), and eqn (1) was used to calculate the rate of degradation of CEES.

$$\eta = \left(\frac{C_0 - C_A}{C_0}\right) \times 100\% \quad (1)$$

where η is the rate of degradation of CEES, C_0 is the initial concentration of CEES, and C_A is the concentration of residual CEES after degradation.

Detection of CEES degradation products

Using methanol as solvent: after placing 5 mg of Al_{13}–TCPP (particle size 500 mesh) in a 50 mL quartz reaction tube, 5 mL of methanol and 5 μL of CEES were added to the tube. After stirring under a 500 W xenon lamp ($\lambda > 400$ nm) and reacting for 180 min, the product of the reaction product was directly analyzed by GC-MS. Using methanol–water solvent mixture (v/v = 1 : 1) as solvent: other steps remained the same, the solvent mixture of methanol and water (5 mL, v/v = 1 : 1) was added as the reaction solvent. After 90 min of reaction, 1 mL of dichloromethane was added to extract the product, and the product was analyzed by GC-MS.

Singlet oxygen and superoxide radical capture experiments

Since 9,10-diphenylanthracene (DPA) is widely used for its ability to specifically capture $^1O_2$, we used highly reactive DPA as an $^1O_2$ trapping agent,[44–46] and H_4TCPP as a reference photosensitizer.[47] H_4TCPP and Al_{13}–TCPP (1×10^{-5} M) were added to 1×10^{-4} M DPA methanol solution and irradiated with the 500 W xenon lamp ($\lambda > 400$ nm). The absorbance values of DPA at the wavelength of 371 nm at different irradiation times were recorded, and the quantum yield of $^1O_2$ was estimated by comparing the slopes of the H_4TCPP and Al_{13}–TCPP linear-square fits (eqn (2)):[46–49]

$$\Phi = \Phi_{Std} \times K/K_{Std} \quad (2)$$

where Φ_{Std} and Φ represent the $^1O_2$ quantum yield of H_4TCPP and Al_{13}–TCPP, respectively, and the $^1O_2$ quantum yield of H_4TCPP in methanol was $\Phi_{TCPP} = 0.135$;[47] K_{Std} and K represent the slope of the absorbance *versus* time curve of DPA degraded by H_4TCPP and Al_{13}–TCPP at the wavelength 371 nm.

The nitroblue tetrazolium (NBT) was used to detect the generation of $O_2^{\bullet-}$, because $O_2^{\bullet-}$ can react with NBT to form formazan, resulting in a decrease in the characteristic absorption peak of NBT at 256 nm.[50,51] Add H_4TCPP and Al_{13}–TCPP (1×10^{-5} M) to the NBT methanol solution of 5×10^{-5} M, and irradiate with the 500 W xenon lamp ($\lambda > 400$ nm). The absorbance values of NBT at the wavelength of 256 nm were recorded for different irradiation times.

Results and discussion

Characterization of Al_{13}–TCPP

The FTIR spectra of H_4TCPP, Al_{13}–SO_4 and Al_{13}–TCPP are shown in Fig. 1. In the FTIR spectrum of H_4TCPP, the band at 1683 cm^{-1} corresponds to the C=O stretching vibration peak of COOH, and the C=C and C=N stretching vibrational peaks of the porphyrin ring at 1596 cm^{-1}. The bands at 1410 cm^{-1} and 1273 cm^{-1} are attributed to the vibration of –OH in COOH, and the band at 961 cm^{-1} is ascribed to the N–H stretching vibration peak of pyrrole.[52,53] In the FTIR spectrum of Al_{13}–TCPP, the characteristic stretching vibration bands of $TCPP^{4-}$ appear at wavenumber 1687, 1602 and 963 cm^{-1}, but there is a slight blue shift compared with the characteristic vibration bands of H_4TCPP. The characteristic stretching vibrational bands at 1410 and 1273 cm^{-1} corresponding to –OH in COOH almost disappear due to the interaction between carboxyl proton and Al_{13}^{7+}. The stretching vibrational bands of Al–O_{Td}, Al–OH and Al–OH_{Oh} in the ε-$[Al_{13}O_4(OH)_{24}(H_2O)_{12}]^{7+}$ cluster are present at 718, 592 and 544 cm^{-1}, respectively.[54,55] Compared with the corresponding characteristic absorption bands at 721, 613 and 549 cm^{-1} of ε $[Al_{13}O_4(OH)_{24}(H_2O)_{12}]^{7+}$ in Al_{13}–SO_4, there is a blue shift to a certain extent, indicating that H_4TCPP and ε-$[Al_{13}O_4(OH)_{24}(H_2O)_{12}]^{7+}$ form a new substance through bond forces.

In the solid-state NMR spectrum of ^{27}Al in Al_{13}–TCPP (Fig. S2†), the spike at the 61.0 ppm chemical shift is ascribed to Al (Al_{Td}) in the Al–O tetrahedron in the center of the Al_{13}^{7+} cationic cluster. The broad peak in the range of −90.5 to 0 ppm chemical shift corresponds to Al (Al_{Oh}) in the 12 Al–O octahedrons in the Al_{13}^{7+} cationic cluster structure. This result is

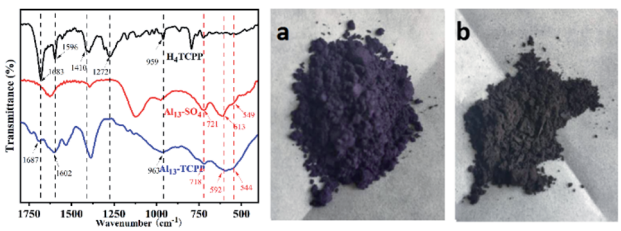

Fig. 1 Infrared spectra of H_4TCPP, Al_{13}–SO_4 and Al_{13}–TCPP (left). Images of H_4TCPP (a) and Al_{13}–TCPP (b) samples (right).

basically consistent with the solid-state NMR shift of ^{27}Al in the Keggin type Al_{13}^{7+} reported in the literature,[56] indicating that the Al_{13}^{7+} in the Al_{13}–TCPP material is indeed an ε-Keggin type structure.

The TG-DTG curve (Fig. S3†) reveals that the weight loss process of Al_{13}–TCPP at room temperature to 800 °C mainly goes through three stages. In the first stage, the weight loss is 10.8% in the range of 25–120 °C, and this part loses 18 crystalline water molecules, with a theoretical value of 9.8%. In the second stage, the weight loss was 25.9% in the range of 120–440 °C, and the loss was due to the water formed by the condensation of the ligand water molecules and the Al–OH–Al group in the anion OH^- and Al_{13}^{7+} cation cluster, with a theoretical value of 28.4%.[57] In the third stage, the weight loss was 20.5% in the range of 440–650 °C, and the organic part of porphyrin TCPP was lost, with a theoretical value of 23.5%. There is no obvious weightlessness peak after 650 °C, and the main compound remaining is Al_2O_3, with an experimental value of 43.8% and a theoretical value of 38.3%. In general, the results of TG analysis (TGA) are basically consistent with the molecular formula obtained by elemental analysis.

The powder XRD pattern of Al_{13}–TCPP shown in Fig. S4† reveals that Al_{13}–TCPP has no obvious characteristic diffraction peak, suggesting that it has an amorphous structure.

Test of the degradation of CEES

In this study, the photocatalytic degradation of the HD simulant CEES by Al_{13}–TCPP in methanol was investigated. As shown in Fig. 2, the degradation rate of CEES increases gradually with the extension of the reaction time. When the reaction time is 180 min, the degradation rate of CEES reaches 96.16%, and with increasing reaction time, the increase of the degradation rate slows down significantly.

In order to further understand the necessity of the active components and photoreaction conditions for the catalytic degradation of CEES in methanol, the degradation of CEES by Al_{13}–TCPP, H_4TCPP and Al_{13}–SO_4 in methanol with or without light was compared. As shown in Fig. 3, when the reaction time is 180 min, the best degradation rate of CEES by Al_{13}–TCPP with light irradiation is 96.16%, but there is almost no degradation without light irradiation, indicating that light irradiation is

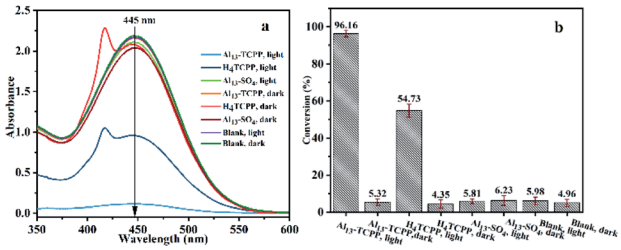

Fig. 3 The UV absorbance (a) and comparison of the performance of Al_{13}–TCPP, H_4TCPP and Al_{13}–SO_4 in the degradation of CEES in methanol (b). Degradation conditions: xenon lamp (λ > 400 nm) at 500 W, reaction time 180 min, solvent: 5 mL methanol, catalyst dosage: Al_{13}–TCPP (5 mg, 1.36 μmol), H_4TCPP (1.2 mg, 1.36 μmol) and Al_{13}–SO_4 (4.3 mg, 3.62 μmol), 5 μL CEES.

a necessary reaction condition for catalytic oxidative degradation of CEES. H_4TCPP is soluble in methanol and undergoes a homogeneous reaction (the absorption peak at the UV wavelength of 420 nm is the Soret band of H_4TCPP).

With light irradiation, the degradation rate of CEES is only 54.73%, which is less than that of Al_{13}–TCPP, indicating that the degradation rate of CEES can be enhanced by the activity of $TCPP^{4-}$ and Al_{13}^{7+} compared with that of H_4TCPP. The degradation rate of CEES by Al_{13}–SO_4 with and without light irradiation is close to that of the blank group, indicating that Al_{13}–SO_4 alone has no obvious ability to degrade CEES.

HD and its simulant CEES can be hydrolyzed in water, but their lipophilic property makes their solubility in water low, which is limited by the mass transfer rate. Adding an organic solvent to water can improve the solubility of CEES in the solvent and increase its hydrolysis rate.[58,59] In order to digest CEES more quickly through hydrolysis, this study further investigated the performance of Al_{13}–TCPP in the degradation of CEES in methanol and water–methanol solvent mixtures (v/v = 1 : 1). As shown in Fig. 4, when other reaction conditions remain unchanged, the results reveal that with the extension of the reaction time, the degradation rate of CEES by Al_{13}–TCPP in solvent mixtures gradually increases, and when the reaction time is 90 min, the degradation rate of CEES reaches 99.01%.

In order to further understand the active components of the materials for the catalytic degradation of CEES in methanol–

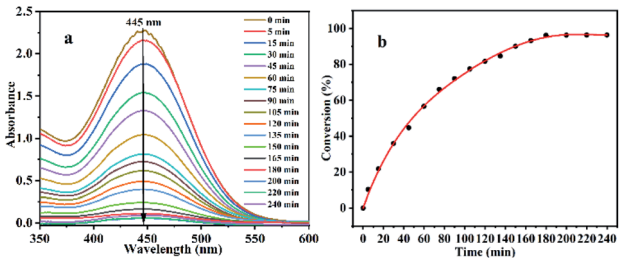

Fig. 2 UV absorption spectra of degradation of CEES by Al_{13}–TCPP at different reaction times (a) and corresponding degradation rate (b). Degradation conditions: 500 W xenon lamp (λ > 400 nm), reaction time 180 min, solvent: 5 mL methanol, catalyst dosage: 5 mg Al_{13}–TCPP, 5 μL CEES.

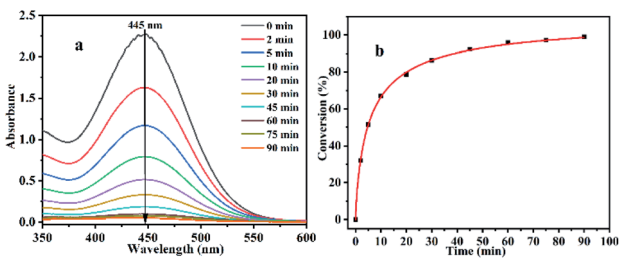

Fig. 4 The UV absorbance (a) and degradation rate (b) of CEES by Al_{13}–TCPP at different reaction times. Degradation conditions: 500 W xenon lamp (λ > 400 nm), reaction time 90 min, reaction solvent: 5 mL methanol and water–methanol solvent mixture (v/v = 1 : 1), catalyst dosage: 5 mg Al_{13}–TCPP, 5 μL CEES.

water solvent mixtures and the requirement of light irradiation in the reaction, the degradation properties of Al_{13}–TCPP, H_4TCPP and Al_{13}–SO_4 in the methanol–water solvent mixtures were compared. As shown in Fig. 5, when the reaction time is 90 min, the degradation rates in methanol–water solvent mixtures in the blank control group with and without light irradiation are 91.06 and 90.32%, respectively, which are almost equal. The best degradation rate of CEES by Al_{13}–TCPP with light irradiation is 99.01%, while the degradation performance without light irradiation (91.46%) is basically equal to that of the blank control group, indicating that light irradiation can promote the catalytic degradation of CEES by Al_{13}–TCPP. The degradation rate of CEES by H_4TCPP with light irradiation is 94.24%, and that without light irradiation is 90.88%, which is lower than that of CEES by Al_{13}–TCPP. $Al_{13}SO_4$ with light irradiation is 90.26%. The degradation rate is basically equal to that of the blank control group in the methanol–water solvent mixture, indicating that $Al_{13}SO_4$ cannot promote the degradation of CEES.

In this study, the kinetics of the catalytic degradation of CEES by Al_{13}–TCPP in methanol and methanol–water solvent mixtures was studied. As shown in Fig. 6, the kinetic curve of the Al_{13}–TCPP degradation of CEES is obtained by fitting the cooperative diagram of the ln (C_{CEES}) to the reaction time, and the result is linear, which shows that the reaction follows first-order kinetics in methanol or in a methanol–water solvent mixture. The kinetic curves show that the half-life and reaction rate constant of Al_{13}–TCPP in the degradation of CEES in methanol and methanol–water solvent mixtures are 39.8 min, -0.047 min^{-1} and 14.7 min, -0.017 min^{-1}, respectively, indicating that the degradation rate of CEES by Al_{13}–TCPP in methanol–water solvent mixtures is much higher than that in methanol.

In this study, the reusability of the catalyst (Al_{13}–TCPP) in the photocatalytic degradation of CEES by Al_{13}–TCPP in a methanol–water solvent mixture was investigated. After each addition of CEES, the reaction was conducted for 90 min, then CEES was added for another 90 minutes, and this process was repeated five consecutive times. As shown in Fig. S5,† the degradation rate was still 98.37% after five reaction cycles, indicating that Al_{13}–TCPP has good reusability.

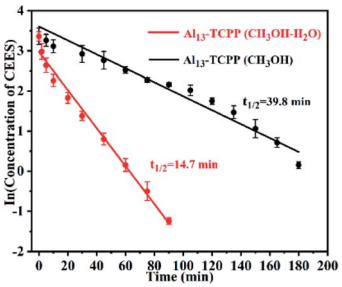

Fig. 6 Kinetic curve of the degradation of CEES by Al_{13}–TCPP in methanol and methanol–water solvent mixture. Degradation conditions: 500 W xenon lamp (λ > 400 nm), reaction time: 180 min in methanol, 90 min in methanol–water solvent mixture, catalyst dosage: 5 mg Al_{13}–TCPP, 5 μL CEES.

In order to study the photocatalytic degradation mechanism of CEES by Al_{13}–TCPP in methanol solvent and methanol–water solvent mixture, the degradation products of CEES were analyzed by GC-MS (Fig. S6 and S7†). As shown in Fig. 7a and b, with light irradiation, CEES undergoes partial alcoholysis in a separate methanol solvent to form 2-methoxyethyl sulfide.[60] A small amount of the hydrolysis product ethyl 2-hydroxyethyl sulfide (HEES) is generated through its hydrolysis and degradation due to the presence of a small amount of water in the solvent.[55,61] When the catalyst Al_{13}–TCPP is added to the methanol solvent, in addition to the formation of 2-methoxyethyl sulfide and a small amount of unreacted CEES, there are two oxidation products, namely ethyl hydroxyethyl sulfoxide (HEESO) and 2-chloroethyl ethyl sulfoxide (CEESO). This may be due to the production of reactive oxygen species (ROS) by Al_{13}–TCPP in the presence of light and oxygen, which selectively oxidizes CEES and HEES into a non-toxic sulfoxide compound.[10,62,63] As shown in Fig. 7c and d, methanol–water solvent mixtures mainly play the role of alcoholysis[60] and

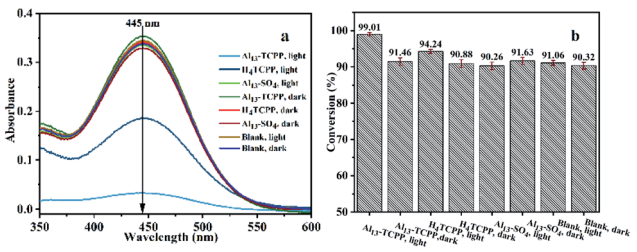

Fig. 5 The UV absorbance (a) and comparison of the performance (b) of Al_{13}–TCPP, H_4TCPP and Al_{13}–SO_4 in the degradation of CEES in methanol–water solvent mixtures. Degradation conditions: 500 W xenon lamp (λ > 400 nm), reaction time 90 min, catalyst dosage: Al_{13}–TCPP (5 mg, 1.36 μmol), H_4TCPP (1.2 mg, 1.36 μmol) and Al_{13}–SO_4 (4.3 mg, 3.62 μmol), 5 μL CEES.

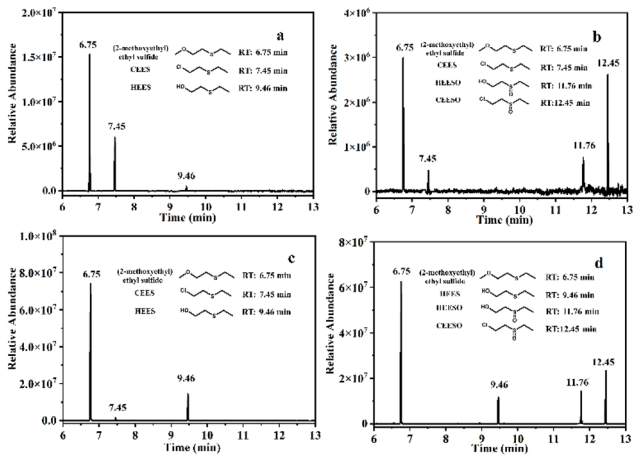

Fig. 7 GC spectra of the products after degradation of CEES in the different solvents (methanol (a and b); methanol–water solvent mixture (c and d)) without (a and c) and with (b and d) Al_{13}–TCPP. Degradation conditions: 500 W xenon lamp (λ > 400 nm), reaction time 180 min, solvent: 5 mL methanol, catalyst dosage: 5 mg Al_{13}–TCPP, 5 μL CEES.

hydrolysis[55,61] on CEES with light irradiation, producing 2-methoxyethyl sulfide and HEES, respectively. In addition to 2-methoxyethyl sulfide and HEES, two new oxidation products, namely HEESO and CEESO, were formed after addition of the methanol–water solvent mixtures to the Al_{13}–TCPP reaction for 90 min. The generation of CEESO is due to the direct oxidation of CEES by ROS produced by Al_{13}–TCPP,[10,64,65] and the generation of HEESO is due to the degradation of CEES by the methanol–water solvent mixture and Al_{13}–TCPP. There are a large number of water molecules in the solvent mixtures, which may first hydrolyze CEES to HEES [48] through the mechanism of sulfur cation intermediate, and then Al_{13}–TCPP produces ROS with light irradiation to continue to oxidize HEES to HEESO.[63]

In order to determine whether the ROS produced by Al_{13}–TCPP degradation of CEES in methanol solvent are singlet oxygen or other kinds, ROS in the reaction process are identified by adding reactive oxygen scavengers. After ROS scavengers and ROS react, the degradation rate of CEES decreases. The methanol solvent itself can be used as a scavenging agent for hydroxyl radicals,[66,67] so the participation of hydroxyl radicals in the degradation of CEES is basically excluded. Therefore, in this experiment $O_2^{\bullet-}$ and $^1O_2$ scavengers were added to determine the types of active oxygen, using benzoquinone as $O_2^{\bullet-}$ scavenger[65] and NaN_3 as $^1O_2$ scavenger.[68] The experimental results listed in Table 1 show that the degradation rate of CEES is 96.16% without scavengers, 54.22 and 53.63% for CEES with benzoquinone or NaN_3, respectively, and 26.53% for CEES with simultaneous addition of benzoquinone and NaN_3, indicating that Al_{13}–TCPP can degrade CEES by producing $O_2^{\bullet-}$ and $^1O_2$ in methanol solvent and with visible light irradiation. According to current reports,[10,62] $^1O_2$ has mild oxidizability, and can selectively oxidize HD and its simulant CEES to non-toxic sulfoxide compounds, while $O_2^{\bullet-}$ can also selectively oxidize sulfides to sulfoxide.[64,65,69,70] Therefore, the hybrid used in this study accelerated the degradation of CEES by using singlet oxygen and superoxide ions produced by porphyrin as oxidants.

In order to determine the $^1O_2$ and $O_2^{\bullet-}$ production abilities of Al_{13}–TCPP, DPA and NBT were used as $^1O_2$ and $O_2^{\bullet-}$ trapping agents, respectively, to capture two reactive oxygen species. As shown in Fig. 8, the absorption value of DPA at the maximum absorption wavelength of 371 nm decreases after the reaction of DPA with $^1O_2$. The quantum yield of $^1O_2$ can be calculated according to the change of the absorption intensity at 371 nm. The experimental results showed that the $^1O_2$ quantum yields of

Table 1 Degradation of CEES by Al_{13}–TCPP in the presence of ROS scavengers[a]

Entry	Reactive oxygen scavenger	Reaction time (min)	Conversion rate (%)
1	None	180	96.16
2	Benzoquinone	180	54.22
3	NaN_3	180	53.63
4	Benzoquinone + NaN_3	180	26.53

[a] Reaction conditions: 500 W xenon lamp ($\lambda > 400$ nm), solvent volume: 5 mL methanol, catalyst dosage: 5 mg Al_{13}–TCPP, benzoquinone (1×10^{-3} M), NaN_3 (1×10^{-2} M), 5 μL CEES, reaction time: 180 min.

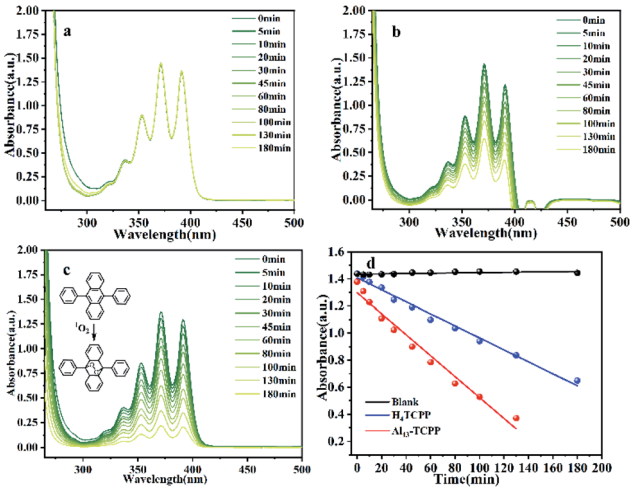

Fig. 8 UV-vis absorption changes of DPA in the presence of Blank (a), H4TCPP (b) and Al_{13}–TCPP (c) under light irradiation with a 500 W xenon lamp ($\lambda > 400$ nm), and the corresponding linear relationship of the absorbance of DPA at the wavelength of $\lambda_{max} = 371$ nm with reaction time (d).

Al_{13}–TCPP and H_4TCPP in methanol are $\Phi = 0.236$ and 0.135, respectively, indicating that, compared with H_4TCPP, the ionic Al_{13}–TCPP hybrid formed by Al_{13}^{7+} and $TCPP^{4-}$ can increase the $^1O_2$ quantum yield, and effectively overcome the problem that porphyrin is prone to self-aggregation in solvent and reduce the quantum yield of $^1O_2$. As shown in Fig. 9, the absorbance changes of NBT in the blank control and H_4TCPP are almost negligible. For the hybrid material Al_{13}–TCPP, the absorbance of NBT at 256 nm gradually decreases with the prolongation of the illumination time, indicating that the Al_{13}–TCPP hybrid can generate $O_2^{\bullet-}$ to participate in CEES oxidative decontamination.

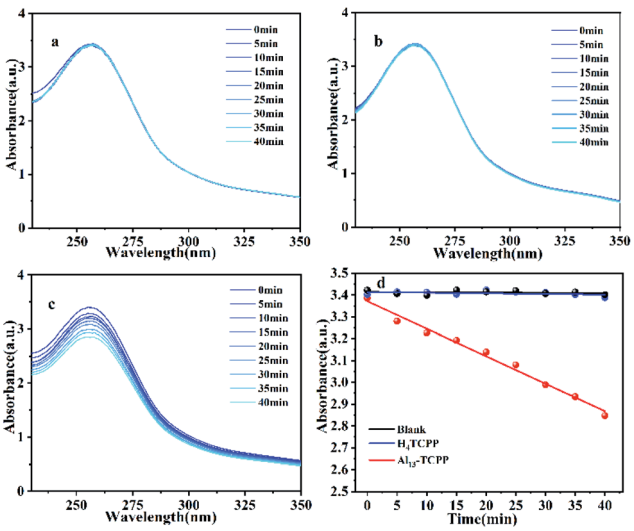

Fig. 9 UV-vis absorption changes of NBT in the presence of Blank (a), H_4TCPP (b) and Al_{13}–TCPP (c) under light irradiation with a 500 W xenon lamp ($\lambda > 400$ nm), and the corresponding linear relationship of the absorbance of NBT at the wavelength of $\lambda_{max} = 371$ nm with reaction time (d).

The above results show that CEES can spontaneously produce different degrees of alcoholysis and hydrolysis in methanol and methanol/water solvent mixtures (the rate is faster with the latter than with the former), resulting in non-toxic HEES and 2-hydroxymethyl ethyl sulfide. In the presence of Al_{13}–TCPP and visible light irradiation, CEES and HEES produce the selective oxidation products HEESO and CEESO (Fig. S8†) caused by the $^1O_2$ and $O_2^{\bullet-}$produced by Al_{13}–TCPPwith light irradiation, thereby speeding up the digestion process.

Table S1† summarizes the performance of some catalysts for the photocatalytic digestion of CEES. Metal–organic frameworks (MOFs) have become the main catalysts for CEES decontamination due to their high stability and fast photocatalytic decontamination efficiency. But it is difficult to prepare in large quantities in a long time and in a short time, and most of the reaction processes need to be fed with pure O_2. At present, most catalysts for degradation of CEES require a greater amount of use than the hybrid materials in this paper. In contrast, the hybrid materials synthesized in this paper have a simple preparation method and can be prepared in large quantities, in the air and visible light irradiation can generate $^1O_2$ and $O_2^{\bullet-}$ to achieve the degradation of CEES.

Conclusion

In this study, a new type of organic–inorganic ionic hybrid material, Al_{13}–TCPP, was prepared. The photocatalytic degradation of CEES by Al_{13}–TCPP in methanol and methanol–water solvent mixture (v/v = 1 : 1) was investigated. The results showed that the degradation rate of CEES was 96.16% in methanol for 180 min and 99.01% in methanol–water solvent mixture for 90 min. The degradation products of CEES were analyzed by GC-MS. The results showed that the degradation of CEES in methanol solvent is achieved through a combination of oxidation and alcoholysis mechanisms. The oxidation mechanism involves the selective oxidation of Al_{13}–TCPP to non-toxic CEESO by using the $O_2^{\bullet-}$ and $^1O_2$ produced by CEES in air and under light irradiation, and Al_{13}–TCPP has a higher quantum yield of $^1O_2$ than H_4TCPP. CEES is degraded through a combination of oxidation, hydrolysis and alcoholysis in the methanol–water solvent mixtures, and the final rapid degradation of CEES is the result of the interaction of Al_{13}–TCPP material and methanol–water solvent mixtures. The material has good reusability and great potential application value in the degradation of HD. Considering the rich and diverse composition, structure, physicochemical properties and binding modes of polyoxometalate and porphyrin, this study provides a successful example for the design of porphyrin–polyoxometalate photosensitive systems with higher $^1O_2$ quantum yield and synergistic effect between polyoxometalate and porphyrin for the efficient degradation of chemical warfare agents.

Conflicts of interest

The authors declare no competing financial interest.

Acknowledgements

The financial support from the Natural Science Foundation of China and kind support from Prof. Xue Duan of Beijing University of Chemical Technology are greatly acknowledged.

Notes and references

1 Y. C. Yang, J. A. Baker and J. R. Ward, *Chem. Rev.*, 1992, **92**, 1729–1743.
2 B. M. Smith, *Chem. Soc. Rev.*, 2008, **37**, 470–478.
3 N. B. Munro, S. S. Talmage, G. D. Griffin, L. C. Waters, A. P. Watson, J. F. King and V. Hauschild, *Environ. Health Perspect.*, 1999, **107**, 933–974.
4 G. W. Wagner, P. W. Bartram, O. Koper and K. J. Klabunde, *J. Phys. Chem. B*, 1999, **103**, 3225–3228.
5 G. W. Wagner, O. B. Koper, E. Lucas, S. Decker and K. J. Klabunde, *J. Phys. Chem. B*, 2000, **104**, 5118–5123.
6 P. Horcajada, S. Surblé, C. Serre, D. Y. Hong, Y. K. Seo, J. S. Chang, J. M. Grenèche, I. Margiolaki and G. r. Férey, *Chem. Commun.*, 2007, 2820–2822.
7 M. J. Geraci, *Ann. Pharmacother.*, 2008, **42**, 237–246.
8 Y. Liu, C. T. Buru, A. J. Howarth, J. J. Mahle, J. H. Buchanan, J. B. DeCoste, J. T. Hupp and O. K. Farha, *J. Mater. Chem. A*, 2016, **4**, 13809–13813.
9 M. Cao, R. Pang, Q. Y. Wang, Z. Han, Z.-Y. Wang, X. Dong, S.-f. Li, S.-q. Zang and T. C. W. Mak, *J. Am. Chem. Soc.*, 2019, **141**, 14505–14509.
10 Y. Liu, S. Y. Moon, J. T. Hupp and O. K. Farha, *ACS Nano*, 2015, **9**, 12358–12364.
11 Z. H. Long, D. Luo, K. Wu, Z. Y. Chen, M. M. Wu, X. P. Zhou and D. Li, *ACS Appl. Mater. Interfaces*, 2021, **13**, 37102–37110.
12 Y. Z. Chen, Z. U. Wang, H. Wang, J. Lu, S. H. Yu and H. L. Jiang, *J. Am. Chem. Soc.*, 2017, **139**, 2035–2044.
13 M. Ethirajan, Y. Chen, P. Joshi and R. K. Pandey, *Chem. Soc. Rev.*, 2011, **40**, 340–362.
14 M. Zhao, S. Ou and C. D. Wu, *Acc. Chem. Res.*, 2014, **47**, 1199–1207.
15 A. Fateeva, P. A. Chater, C. P. Ireland, A. Tahir, Y. Z. Khimyak, P. V. Wiper, J. R. Darwent and M. J. Rosseinsky, *Angew. Chem., Int. Ed.*, 2012, **51**, 7440–7444.
16 C. Tanielian, C. Wolff and M. Esch, *J. Phys. Chem.*, 1996, **100**, 6555–6560.
17 C. Tanlelian, C. Schwweitzer, R. Mechin and C. Wolff, *Free Radical Biol. Med.*, 2001, **30**, 208–212.
18 Y. Zhang, J. Ma, D. Wang, C. Xu, S. Sheng, J. Cheng, C. Bao, Y. Li and H. Tian, *Biomater. Sci.*, 2020, **8**, 6526–6532.
19 D. Wang, L. Niu, Z.-Y. Qiao, D.-B. Cheng, J. Wang, Y. Zhong, F. Bai, H. Wang and H. Fan, *ACS Nano*, 2018, **12**, 3796–3803.
20 Y. Liu, A. J. Howarth, J. T. Hupp and O. K. Farha, *Angew. Chem., Int. Ed.*, 2015, **54**, 9001–9005.
21 C. T. Buru, M. B. Majewski, A. J. Howarth, R. H. Lavroff, C.-W. Kung, A. W. Peters, S. Goswami and O. K. Farha, *ACS Appl. Mater. Interfaces*, 2018, **10**, 23802–23806.
22 M.-H. Xie, X.-L. Yang, C. Zou and C.-D. Wu, *Inorg. Chem.*, 2011, **50**, 5318–5320.

23 Z. H. Zhu, Y. Liu, C. Song, Y. Hu, G. Feng and B. Z. Tang, *ACS Nano*, 2021, **16**, 1346–1357.
24 C. F. Pereira, Y. Liu, A. Howarth, F. Figueira, J. Rocha, J. T. Hupp, O. K. Farha, J. P. C. Tomé and F. A. Almeida Paz, *ACS Appl. Nano Mater.*, 2018, **2**, 465–469.
25 C. L. Hill, *Mol. Catal.*, 1996, **114**, 1–3.
26 C. L. Hill and C. M. McCartha, *Coord. Chem. Rev.*, 1995, **143**, 407–455.
27 J. Alcañiz-Monge, G. Trautwein, S. Parres-Esclapez and J. A. Maciá-Agulló, *Microporous Mesoporous Mater.*, 2008, **115**, 440–446.
28 H. M. Asif, N. Qu, Y. Zhou, L. Zhang, F. K. Shehzad, Z. Shi, Y. Long and S. U. Hassan, *Inorg. Chem. Front.*, 2017, **4**, 1900–1908.
29 C. L. Hill, *Chem. Rev.*, 1998, **98**, 1–2.
30 D. Schaming, C. e. Allain, R. Farha, A. Giraudeau, B. Hasenknopf, L. Ruhlmann, M. Goldmann and S. Lobstein, *Langmuir*, 2010, **26**, 5101–5109.
31 T. Ishizuka, S. Ohkawa, H. Ochiai, M. Hashimoto, K. Ohkubo, H. Kotani, M. Sadakane, S. Fukuzumic and T. Kojima, *Green Chem.*, 2018, **20**, 1975–1980.
32 G. Zhu, Y. Long, H. Ren, Y. Zhou, L. Zhang, Z. Shi, F. K. Shehzad and H. M. Asif, *J. Phys. Chem. C*, 2016, **120**, 22549–22557.
33 S. u. Hassan, Y. Zhou, L. Zhang, Z. Shi, D. Yang, H. M. Asif and N. Qu, *J. Phys. Chem. C*, 2016, **120**, 7757–7766.
34 Y. Wu, J. Dong, C. Liu, X. Jing, H. Liu, Y. Guo, Y. Chi and C. Hu, *Dalton Trans.*, 2021, **50**, 9796–9803.
35 X. Zhang, Y. Li, Y. Li, S. Wang and X. Wang, *ACS Appl. Nano Mater.*, 2019, **2**, 6971–6981.
36 S. u. Hassan, Y. Zhou, L. Zhang, Z. Shi, D. Yang, H. M. Asif and N. Qu, *Inorg. Chem.*, 2020, **59**, 2575–2583.
37 P. D. Bartlett and C. G. Swain, *J. Am. Chem. Soc.*, 1949, **71**, 1406–1415.
38 R. I. Tilley, *Aust. J. Chem.*, 1993, **46**, 293–300.
39 C. Ye, Y. Zhang, A. Ding, Y. Hu and H. Guo, *Sci. Rep.*, 2018, **8**, 2205–2210.
40 F. Fringuelli, R. Pellegrino and F. Pizzo, *Synth. Commun.*, 2006, **23**, 3157–3163.
41 X. Gu, X. Li, Y. Chai, Q. Yang, P. Li and Y. Yao, *Green Chem.*, 2013, **15**, 357–361.
42 J. S. Lindsey and R. W. Wagner, *J. Org. Chem.*, 1989, **54**, 828–836.
43 M. Wang and M. Muhammed, *Nanostruct. Mater.*, 1999, **11**, 1219–1229.
44 T. Nakazono, A. R. Parent and K. Sakai, *Chemistry*, 2015, **21**, 6723–6726.
45 C. Mongin, A. M. Ardoy, R. Mereau, D. M. Bassani and B. Bibal, *Chem. Sci.*, 2020, **11**, 1478–1484.
46 N. Zheng, Z. Zhang, J. Kuang, C. Wang, Y. Zheng, Q. Lu, Y. Bai, Y. Li, A. Wang and W. Song, *ACS Appl. Mater. Interfaces*, 2019, **11**, 18224–18232.
47 S. Liu, Y. Hua, C. Hua, Y. Xiong and M. Duan, *J. Porphyrins Phthalocyanines*, 2019, **23**, 1084–1091.
48 J. Jin, Y. Zhu, Z. Zhang and W. Zhang, *Angew. Chem., Int. Ed.*, 2018, **57**, 16354–16358.
49 F. Nifiatis, J. C. Athas, K. D. D. Gunaratne, Y. Gurung, K. M. Monette and P. J. Shivokevich, *Open Spectrosc. J.*, 2011, **5**, 1–12.
50 Y. Zhao, X. Liang, H. Shi, Y. Wang, Y. Ren, E. Liu, X. Zhang, J. Fan and X. Hu, *Chem. Eng. J.*, 2018, **353**, 56–68.
51 H. Shi, J. Fan, Y. Zhao, X. Hu, X. Zhang and Z. Tang, *J. Hazard. Mater.*, 2020, **381**, 121006.
52 B. Zhuanga, X. Lia, R. Gea, S. Kanga, L. Qina and G. Lib, *Appl. Catal., A*, 2017, **533**, 81–89.
53 N. Sadeghia, S. Sharifniaa and M. S. Arabib, *J. CO2 Util.*, 2016, **16**, 450–457.
54 C. M. Flynn Jr and T. Pope, *Inorg. Chem.*, 1971, **10**, 2524–2529.
55 J. H. Son and Y. U. Kwon, *Inorg. Chem.*, 2004, **43**, 1929–1932.
56 J. H. Son, H. Choi, Y.-U. Kwon and O. H. Han, *J. Non-Cryst. Solids*, 2003, **318**(1–2), 186–192.
57 J.-H. Son, H. Choi and Y.-U. Kwon, *J. Am. Chem. Soc.*, 2000, **122**(30), 7432–7433.
58 P. D. Bartlett and C. G. Swain, *J. Am. Chem. Soc.*, 1948, **71**, 1406–1415.
59 R. I. Tilley, *Aust. J. Chem.*, 1993, **46**(3), 293–300.
60 R. M. Narske, K. J. Klabunde and S. Fultz, *Langmuir*, 2002, **18**, 4819–4825.
61 J. T. Kloprogge, H. Ruan and R. L. Frost, *J. Mater. Sci.*, 2001, **36**, 603–607.
62 C. Changtonga, D. W. Carneya, L. Luoa, C. A. Zotoa, J. L. Lombardib and R. E. Connorsa, *J. Photochem. Photobiol., A*, 2013, **260**, 9–13.
63 L. J. Chen, S. Chen, Y. Qin, L. Xu, G. Q. Yin, J. Zhu, F. F. Zhu, W. Zheng, X. Li and H.-B. Yang, *J. Am. Chem. Soc.*, 2018, **140**, 5049–5052.
64 J. Jiang, R. Luo, X. Zhou, Y. Chen and H. Jia, *Adv. Synth. Catal.*, 2018, **360**, 4402–4411.
65 H. Guo, H. Xia, X. Ma, K. Chen, C. Dang, J. Zhao and B. Dick, *ACS Omega*, 2020, **5**, 10586–10595.
66 J. S. Daniels and K. S. Gates, *J. Am. Chem. Soc.*, 1996, **118**(14), 3380–3385.
67 J. T. Schneider, D. S. Firak, R. R. Ribeiro and P. PeraltaZamora, *Phys. Chem. Chem. Phys.*, 2020, **22**, 15723–15733.
68 M. Scholz, R. Dědic, T. Breitenbach and J. Hála, *Photochem. Photobiol. Sci.*, 2013, **12**, 1873–1884.
69 J. Jiang, R. Luo, X. Zhou, Y. Chen and H. Ji, *Adv. Synth. Catal.*, 2018, **360**, 4402–4411.
70 E. L. Clennan, *Acc. Chem. Res.*, 2001, **34**, 875–884.